PHOTONICS Research

Enhanced magneto-optical Kerr effect and index sensitivity in Au/Fe_xCo_{1-x} magnetoplasmonic transducers

Haipeng Lu,[1,2] Chuan Liu,[1,2] Jun Qin,[1,2] Chuangtang Wang,[1,2] Yan Zhang,[1,2] Longjiang Deng,[1,2] and Lei Bi[1,2,*]

[1]National Engineering Research Center of Electromagnetic Radiation Control Materials, University of Electronic Science and Technology of China, Chengdu 610054, China
[2]School of Microelectronics and Solid State Electronics, University of Electronic Science and Technology of China, Chengdu 610054, China
*Corresponding author: bilei@uestc.edu.cn

Received 13 April 2017; revised 7 June 2017; accepted 20 June 2017; posted 21 June 2017 (Doc. ID 292686); published 2 August 2017

Magnetoplasmonic sensors are attractive candidates for ultrasensitive chemical and biomedical sensor applications. A variety of ferromagnetic metal thin films have been used for magnetoplasmonic device applications, yet the dependence of sensor performance on the optical and magneto-optical properties of ferromagnetic metal materials has been rarely studied. In this work, we report the study of enhanced magneto-optical Kerr effect (MOKE) and sensing performance in Au/Fe_xCo_{1-x} bilayer magneto-optical surface plasmon resonance (MOSPR) transducers. The optical constants of Fe_xCo_{1-x} ($x = 0$, 0.29, 0.47, 0.65, and 1) in a sputter-deposited Au/Fe_xCo_{1-x} device are characterized by the attenuated total internal reflection (ATR) method. Fe_xCo_{1-x} thin films show different MOKEs as a function of the chemical concentration, with the highest transverse MOKE signal observed in $Fe_{0.7}Co_{0.3}$. Index sensing performance is closely related to the material's optical and magneto-optical constants. By studying the sensing performance in the parameter space of the Au/Fe_xCo_{1-x} bilayer thicknesses, the highest sensitivity is found to be 0.385 (theoretical) and 0.306 RIU^{-1} (experimental) in the Au/$Fe_{0.7}Co_{0.3}$ MOSPR devices. Our research highlights the influence of the optical properties of ferromagnetic material to device sensitivity in MOSPR transducers. The high sensitivity in Au/Fe_xCo_{1-x} MOSPR devices make these structures attractive candidates for chemical and biomedical sensing applications.

OCIS codes: (280.0280) Remote sensing and sensors; (240.6680) Surface plasmons; (160.3820) Magneto-optical materials.

https://doi.org/10.1364/PRJ.5.000385

1. INTRODUCTION

Surface plasmon resonance (SPR) sensors, which utilize the collective oscillation of electrons at the interface between a metal and a dielectric thin film, are promising candidates for ultrasensitive chemical and biomedical sensing applications. Because of the high optical loss of noble metals used in SPR sensors, the limits of detection (LODs) of SPR devices based on intensity modulation are usually in the range of 10^{-5} – 10^{-6} refractive index unit (RIU) [1,2]. To further improve device sensitivity, magneto-optical SPR (MOSPR) devices are developed. Such a device introduces a ferromagnetic thin film such as cobalt into the SPR structure. The highly confined electromagnetic field caused by SPR can also lead to a significantly enhanced transverse magneto-optical Kerr effect (TMOKE) in the Co layer, which can be utilized to modulate the SPR resonance condition with applied magnetic fields. Because of the high absorption loss of the ferromagnetic metal thin films, a noble metal/ferromagnetic metal multilayer structure is usually applied in MOSPR sensors. For example, Au/Co multilayer MOSPR transducers have been demonstrated to show 3 times higher sensitivity experimentally compared to conventional SPR sensors [3], whereas a potential 1 order of magnitude improvement of the device sensitivity has been predicted theoretically [3].

Several methods that consider the fundamental trade-off between the high magneto-optical response and low loss of an MOSPR transducer have been proposed to improve the sensitivity of MOSPR devices. One way to achieve this is to optimize the noble metal and ferromagnetic metal layers' thicknesses and positions, which influence the modal distribution in the ferromagnetic metal layer of the MOSPR device [4–7]. Another way is to use noble metal materials with lower optical loss, such as using Ag instead of Au, to introduce lower optical absorption in the MOSPR device [8]. On the other hand, several different magnetic metal thin films are applied for MOSPR devices, such as Fe, Co, NiFe (Permalloy), and IrMn [8–14]. However, there are very few reports that study

the influence of different magnetic metals on device performance. For example, a much higher magneto-optical coefficient has been observed in Fe compared to Co at 650 nm wavelength [15], while the optical loss of Fe is much higher. How the optical and magneto-optical properties of the magnetic metal thin films would influence device performance is unclear. Therefore, exploring novel ferromagnetic metal materials with different optical and magneto-optical properties may also improve the performance of MOSPR sensors.

In this work, we report a study on the optical and magneto-optical properties of Fe_xCo_{1-x} ($x = 0$, 0.29, 0.47, 0.65, and 1) thin films in an Au/Fe_xCo_{1-x} bilayer structure for MOSPR sensor applications. We observed that when doping Fe with Co, the magneto-optical effect of Fe_xCo_{1-x} first increases and then decreases with further increase in Co concentrations [15]. Meanwhile, the optical constants of Fe_xCo_{1-x} vary with the compositions, leading to lower optical loss with higher Co doping concentration. The highest sensitivity for all Fe_xCo_{1-x} concentrations studied is observed in $Au/Fe_{0.7}Co_{0.3}$ MOSPR transducers, which is mostly due to the highest magneto-optical effect of $Fe_{0.7}Co_{0.3}$, indicating a promising potential for using these devices for chemical and biomedical sensing applications.

The paper is arranged as follows. In Section 2, we introduce the simulation and experimental methods. In Section 3, we report the structure and optical and magneto-optical properties of sputter deposited Fe_xCo_{1-x} thin films in an Au/Fe_xCo_{1-x} bilayer structure deposited on glass substrates. The full permittivity tensors of Fe_xCo_{1-x} thin films are characterized at 650 nm wavelength. Then, based on the characterized material properties, the performance of Au/Fe_xCo_{1-x} plasmonic sensors as a function of the device geometry is presented. Finally, devices with the optimum geometries for Au/Fe, $Au/Fe_{0.7}Co_{0.3}$, and Au/Co bilayer structures are fabricated for TMOKE spectrum characterizations and index sensing experiments in water-based solutions. The experimental results are then compared with theoretical calculations.

2. SIMULATION AND EXPERIMENTAL METHODS

A. Deposition and Characterization Methods for Fe_xCo_{1-x} Thin Films

Fe_xCo_{1-x} thin films were prepared by magnetron co-sputtering of Fe ($\Phi = 2''$, Alfa Aesa, 99.9%) and Co ($\Phi = 2''$, Alfa Aesa, 99.9%) targets on BK7 glass substrates at room temperature. Because of the high magnetization of Fe, to make sure Fe target and Co target can ignite under the same Ar pressure, the thickness of Fe target is 0.67 mm which is about one third of Co target's 2 mm. Before the deposition process, the sputtering chamber was pumped down to a base pressure of 1×10^{-4} Pa. For the best film quality, we controlled the Ar pressure to be 0.5 Pa for all depositions. The chemical composition of the thin films (thickness around 18 nm) were controlled by varying the sputtering power of the Fe and Co targets from 0 to 50 W, which yields Fe_xCo_{1-x} thin film compositions of $x = 1.0$, 0.65, 0.47, 0.29, and 0 as determined by energy dispersive spectroscopy (EDS) and also calibrated by a standard $Fe_{0.5}Co_{0.5}$ sample with known stoichiometry. The crystal structures of all films were characterized by X-ray diffraction (XRD) on a Shimadzu XRD7000 X-ray diffractometer. For optical constant characterization, 12–18 nm Fe_xCo_{1-x} thin films were first deposited on BK7 glass substrates. Then an Au thin-film layer with thickness of 18 nm was deposited on top of Fe_xCo_{1-x} thin films by direct current (DC) sputtering at room temperature to form the Au/Fe_xCo_{1-x} bilayer structure. The reflectivity spectrum as a function of the incident angle of a CW laser operating at 650 nm wavelength is collected with 0 applied magnetic fields. By applying the transfer matrix method and adopting a least square fitting procedure to the reflectivity spectrum, the optical constants of Fe_xCo_{1-x} thin films are obtained. In order to avoid the interference effect in thin films (<100 nm), optically opaque thin films (200 nm) of Fe_xCo_{1-x} are deposited at the same conditions as the bilayer structure for longitudinal magneto-optical Kerr effect (LMOKE) characterizations. The Kerr rotation angle and Kerr ellipticity for all thin films were characterized on a microscopic magneto-optical Kerr effect (MOKE) characterization system with incident laser wavelength of 650 nm at a fixed incident angle of 45°. The off-diagonal components and full dielectric tensor of Fe_xCo_{1-x} thin films at 650 nm wavelength were characterized by LMOKE and reflectivity characterizations.

B. TMOKE Spectrum and Refractive Index Sensing Characterizations of Au/Fe_xCo_{1-x} MOSPR Sensors

The MOSPR sensor structure studied in this paper is shown in Fig. 1. A prism coupling setup with Kretschmann configuration is used to excite the SPR using the attenuated total internal reflection (ATR) method. An index matching refractive index liquid ($n = 1.52$) is applied between the substrates and a BK7 glass prism. The prism and MOSPR sensor device is placed on a $\theta - 2\theta$ rotation stage driven by step motors with an angle resolution of 0.001°. A semiconductor laser operating at 650 nm wavelength is incident from the prism side on the substrate/metal-thin-film interface. SPR is excited at a θ_{SPR} angle when the phase matching condition is met. The magnetic field (2000 Oe) is applied perpendicular to the incident plane, i.e., along the y axis in Fig. 1. The propagation constant of the

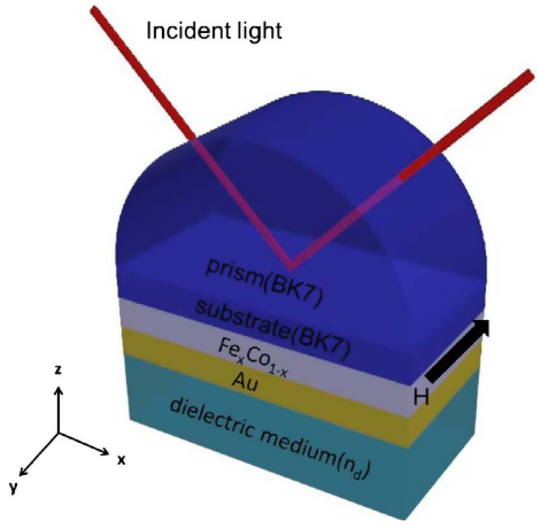

Fig. 1. Schematic view of the Au/Fe_xCo_{1-x} MOSPR sensor in a Kretschmann prism coupling system. The external magnetic field is applied along the y axis and perpendicular to the incident plane.

SPR mode is modulated by the applied magnetic field, which leads to an enhanced TMOKE signal. The sensitivity of the MOSPR sensor is defined as

$$S = \frac{\partial(R(+H) - R(-H))}{\partial\theta} \times \frac{\partial\theta}{\partial n} = \frac{\partial\Delta R}{\partial n}, \quad (1)$$

where $R(+H)$ and $R(-H)$ stand for the reflectivity of light at positive or negative applied magnetic fields, respectively, θ is the incident angle, and n is the refractive index of the dielectric sensing medium. To evaluate the device sensitivity, the 4 × 4 transfer matrix method was applied to study the reflectivity and TMOKE spectrum of Au/Fe_xCo_{1-x} devices under in-plane applied magnetic fields [16], where the prism coupled Au/Fe_xCo_{1-x} system is treated as a four layer system with the first layer to the fourth layer as prism (substrate), Fe_xCo_{1-x}, Au, and the dielectric sensing medium, respectively. The optimum sensor geometry with maximum sensitivity S is determined by simulating Eq. (1) using the method described above and exploring the parameter space of Au and Fe_xCo_{1-x} thicknesses. This optimum device geometry is then fabricated for index sensing experiments and compared with the theoretical results.

3. RESULTS AND DISCUSSION

A. Structure and Optical and Magneto-Optical Properties of Fe_xCo_{1-x} Thin Films

Figure 2(a) shows the XRD patterns of Fe_xCo_{1-x} thin films (~18 nm) deposited on BK-7 glass substrates in the 2θ range of 40°–50°. A full range XRD scan for the $Fe_{0.7}Co_{0.3}$ thin film is also shown in the inset All Fe_xCo_{1-x} thin films are well crystallized. Because we deposit all samples at room temperature without any annealing process, the pure Co thin film shows the hexagonal close-packed (HCP) phase [17], whereas all Fe_xCo_{1-x} thin films with $x > 0$ show the body-centered cubic (BCC) phase [18]. The Fe_xCo_{1-x} thin films with $0 < x < 1$ form a BCC phase, which is similar to reports in previous studies [19,20]. With increasing x, the characteristic (110) diffraction peak of the Fe_xCo_{1-x} thin films shifts to lower 2θ angles, indicating a solid solution behavior.

To characterize the optical constants of Fe_xCo_{1-x} thin films in an Au/Fe_xCo_{1-x} MOSPR device structure, we measured the reflectivity spectrum of the MOSPR transducers using prism coupling via the angular interrogation method. The Au and Fe_xCo_{1-x} thicknesses are both fixed at 18 nm for different samples. Figure 2(b) shows the reflectivity spectrum for Au/Fe, Au/$Fe_{0.7}Co_{0.3}$, and Au/Co samples. Surface plasmon polaritons are excited in all three structures, as indicated by the broad SPR peaks at around 45°. We used the least square method to fit the experimental spectrum with the calculated spectrum by using the transfer matrix method by fixing the Au and Fe_xCo_{1-x} layer thicknesses and varying the Fe_xCo_{1-x} thin films' optical constants, therefore obtaining the fitted n, k values of Fe_xCo_{1-x} thin films at a 650 nm wavelength. The experimental and fitted reflection spectrum of the Au(18 nm)/$Fe_{0.7}Co_{0.3}$(18 nm) sample is shown in the inset of Fig. 2(b). Similarly, the diagonal component of the permittivity tensor of Fe_xCo_{1-x} and Fe are obtained as shown in Table 1. We noticed that Fe and Fe_xCo_{1-x} thin films showed higher optical loss than Co, which resulted in larger FWHM in the reflectivity spectrum. This trend is consistent with the optical constants of Fe_xCo_{1-x} thin films from literature reports [21,22], despite of a much thinner film thickness in our samples compared to previous studies.

To characterize the off-diagonal component of the Fe_xCo_{1-x} thin films, the LMOKE spectrum was measured on optically opaque (200 nm) Fe_xCo_{1-x} thin films deposited on glass substrates at 650 nm wavelength. Figure 3(a) shows room temperature LMOKE hysteresis of Co, $Fe_{0.7}Co_{0.3}$ and Fe thin films. The Kerr rotation and Kerr ellipticity for all samples are plotted in Fig. 3(b). The error bars are generated by accounting for the standard deviation of five measurements for each Fe_xCo_{1-x} sample. The Kerr rotation angle of Fe_xCo_{1-x} thin films first increases with x, peaks at $Fe_{0.7}Co_{0.3}$, and then decreases for the pure Fe. The Kerr ellipticity, on the other hand, reaches

Table 1. Dielectric Tensor Elements of Fe, Fe_xCo_{1-x}, and Co Thin Films Deposited on Glass Substrates[a]

Magneto-Optical Thin Films	ε'_{xx}	ε''_{xx}	ε'_{xz}	ε''_{xz}
Fe	−0.86	16.52	−0.430(±0.009)	0.142(±0.011)
$Fe_{0.7}Co_{0.3}$	−0.72	17.87	−0.518(±0.010)	0.288(±0.012)
$Fe_{0.5}Co_{0.5}$	−1.05	17.04	−0.464(±0.011)	0.273(±0.013)
$Fe_{0.3}Co_{0.7}$	−0.97	16.42	−0.403(±0.017)	0.268(±0.018)
Co	−9.72	21.11	−0.404(±0.012)	0.0015(±0.016)

[a]The error bars of ε'_{xz} and ε''_{xz} are determined by the standard deviation of LMOKE measurements from multiple measurements.

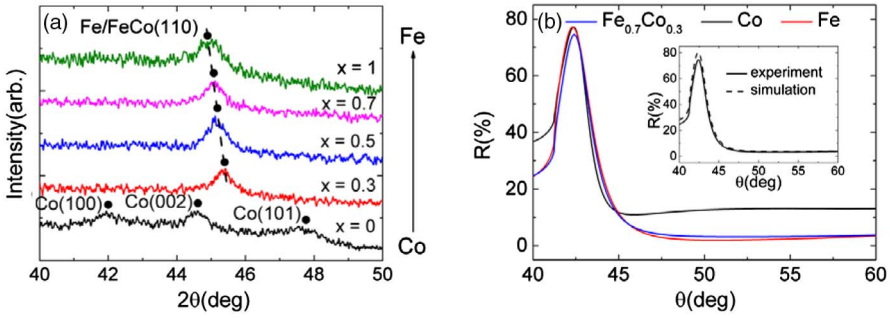

Fig. 2. (a) XRD figures of different component Fe_xCo_{1-x} samples with about 18 nm thickness. (b) Reflectivity versus incidence angle for the Au(18 nm)/Fe/Co/$Fe_{0.7}Co_{0.3}$(18 nm) device; the inset shows the simulated result (dashed line) compared to the experimental curve (solid line) of Au(18 nm)/$Fe_{0.7}Co_{0.3}$(18 nm). The reflectivity spectra are measured in air.

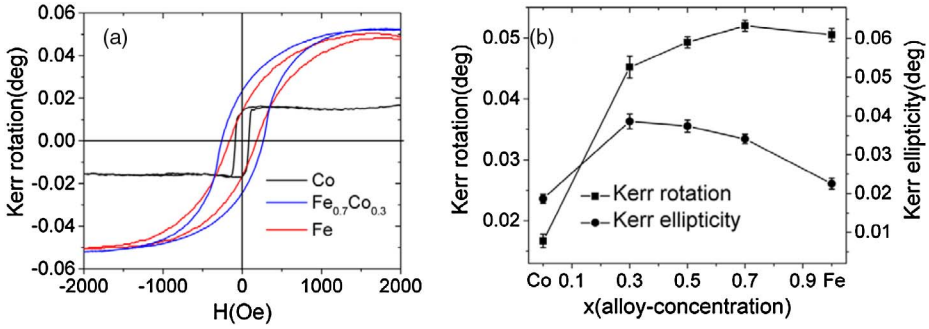

Fig. 3. (a) Room temperature LMOKE hysteresis of Fe_xCo_{1-x} thin films measured under an incident laser wavelength of 650 nm. (b) The LMOKE Kerr rotation and Kerr ellipticity of Fe_xCo_{1-x} thin films with different composition x.

the maximum at the composition of $Fe_{0.3}Co_{0.7}$. The off-diagonal elements of the permittivity tensor can be calculated from the longitude Kerr rotation and ellipticity using the following equations [23]:

$$\Theta_K = \mathrm{Re}\frac{(\pm r_{sp})}{r_{ss}(r_{pp})} = \mathrm{Im}\frac{\sin\varphi\eta^2[\sin\varphi\tan\varphi \pm (\eta^2-\sin^2\varphi)^{1/2}]}{(\eta^2-1)(\eta^2-\tan^2\varphi)(\eta^2-\sin^2\varphi)^{1/2}}Q, \tag{2}$$

$$\psi_K = \mathrm{Im}\frac{(\pm r_{sp})}{r_{ss}(r_{pp})} = \mathrm{Re}\frac{\sin\varphi\eta^2\left[\sin\varphi\tan\varphi \pm (\eta^2-\sin^2\varphi)^{1/2}\right]}{(\eta^2-1)(\eta^2-\tan^2\varphi)(\eta^2-\sin^2\varphi)^{1/2}}Q, \tag{3}$$

where Θ_K is the magneto-optical Kerr rotation angle, ψ_K is the magneto-optical Kerr ellipticity, and $\eta = n_2/n_1$ represents the complex refraction index ratio between air (n_1) and Fe_xCo_{1-x} (n_2). The r_{sp}, r_{ss}, and r_{pp} terms are reflectivity of s-polarized, s-polarized, and p-polarized light, with p-polarized, s-polarized and p-polarized incident light, respectively. φ is the incidence angle with respect to the film surface normal, and Q is the Voigt constant, which was solved from the equations. Using the measured MOKE angle, ellipticity and the thin-film optical constants, the off-diagonal elements can be calculated as

$$\varepsilon_{xz} = i * \varepsilon_{xx} * Q. \tag{4}$$

The result is also shown in Table 1. For both the real and imaginary part of the off-diagonal component of the permittivity tensor, they first increase with Fe concentration, maximize at $Fe_{0.7}Co_{0.3}$, and then decrease for pure Fe. This trend agrees with the literature reports on epitaxial Fe_xCo_{1-x} thin films [15].

B. Index Sensitivity of Au/Fe_xCo_{1-x} MOSPR Transducers

Next we evaluate the sensitivity of Au/Fe_xCo_{1-x} MOSPR transducers as index sensors. The device sensitivity is first simulated numerically according to Eq. (1) in the parameter space of Au and Fe_xCo_{1-x} thin-film thicknesses. A typical simulation result for the Au/Co transducer is shown in Fig. 4(a). Optimum device geometry is observed with Co and Au layer thicknesses of 13 and 38 nm, respectively. This observation can be understood as a result of the trade-off between the MO effect and the optical absorption in Au/Fe_xCo_{1-x} devices [6]. In the case of Fe and Fe_xCo_{1-x}, the optimum Au layer becomes a little thicker, which is due to the higher loss and higher index in Fe rich Fe_xCo_{1-x} thin films. The maximum sensitivity of each Au/Fe_xCo_{1-x} MOSPR transducer is shown in Fig. 4(b); the Au/$Fe_{0.7}Co_{0.3}$ device show the highest sensitivity of $0.385 \pm 0.008\ \mathrm{RIU}^{-1}$, mostly due to its highest MO effect. The error bar in the sensitivity value is from the error bar in determination of the Fe_xCo_{1-x}'s off-diagonal component.

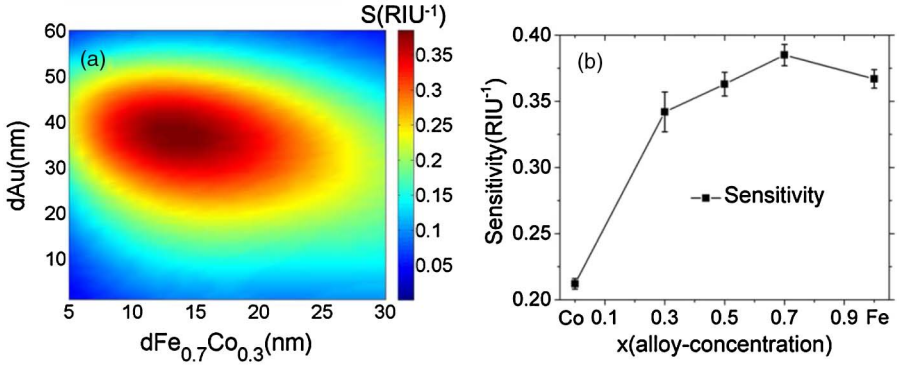

Fig. 4. (a) Simulated device sensitivity as a function of Au and Co layer thicknesses in the Au/Co transducer. (b) The optimum sensitivity of Au/Fe_xCo_{1-x} MOSPR transducers with different composition x; the error bar of sensitivity is determined by the error bar of ε'_{xz} and ε''_{xz} as shown in Table 1.

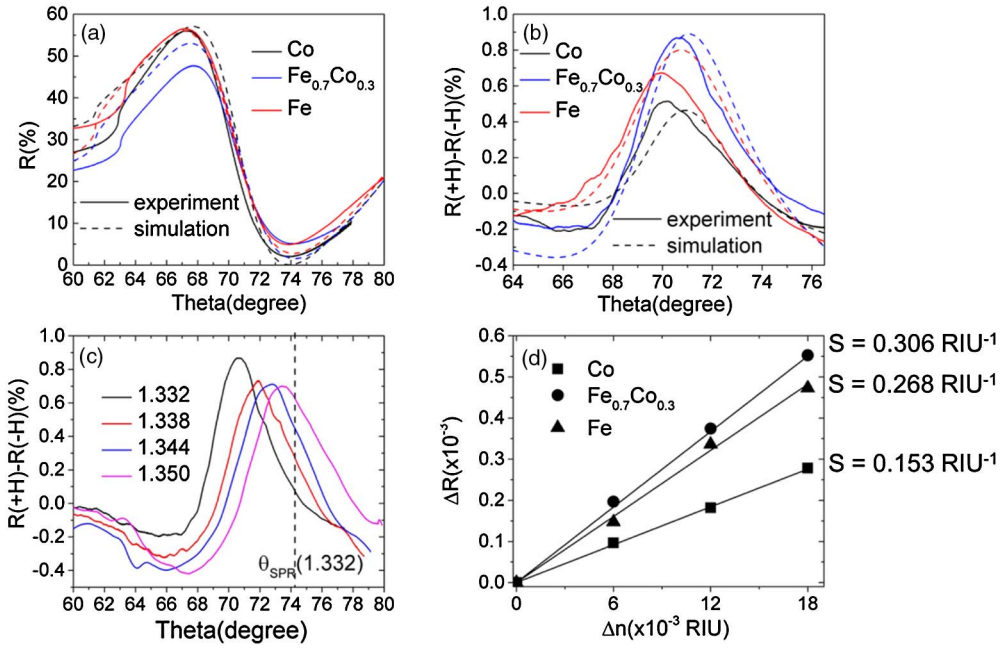

Fig. 5. (a) Experimental and simulated angular spectrum of R for p-polarized incident light in three Au/Fe_xCo_{1-x} MOSPR transducers measured in water ($n = 1.332$) (b) Experimental and simulated angular spectrum of $R(+H) - R(-H)$ for p-polarized incident light in three $Au/Fe_{0.7}Co_{0.3}$ MOSPR transducers. (c) Experimental angular spectrum of $R(+H) - R(-H)$ as a function of the index of the sensing medium for the $Au/Fe_{0.7}Co_{0.3}$ transducer. (d) Comparison of the index sensitivity for Au/Fe, $Au/Fe_{0.7}Co_{0.3}$ and Au/Co devices as a function of the index of the sensing medium.

The optimum device structure for Au/Fe, $Au/Fe_{0.7}Co_{0.3}$, and Au/Co devices are then fabricated for index sensing experiments. The reflectivity spectra of all three devices are characterized as a function of the light incident angle, as shown in Fig. 5(a) by the ATR method measured in water ($n = 1.332$). The spectra feature reflectivity minima at around 74°, which corresponds to SPR excitation in all MOSPR transducers. The simulated reflectivity spectrum agrees with the experimental spectrum very well. By measuring the $R(+H) - R(-H)$ spectrum as a function of incidence angle, clear TMOKE enhancement due to SPR excitation is observed for all devices, as shown in Fig. 5(b). The numerical simulation results using the material optical constants shown in Table 1 also agree well with the experimental spectra. The highest TMOKE is observed in the $Au/Fe_{0.7}Co_{0.3}$ sample, which is consistent with the strongest magneto-optical effect observed in this material. Index sensing performance of the three devices of Au/Fe, Au/Co, and $Au/Fe_{0.7}Co_{0.3}$ are characterized, with the example TMOKE spectrum of the $Au/Fe_{0.7}Co_{0.3}$ transducer as a function of the solution index of refraction, as shown in Fig. 5(c). With increasing the solution index, the TMOKE spectrum gradually shifts to higher angles, which is due to the larger effective index of the excited SPR modes. As shown in Fig. 5(d), all three MOSPR devices show good linearity as a function of the solution index for a large range of refractive indices. The highest sensitivity of $0.306 \pm 0.008\ RIU^{-1}$ is observed in the $Au/Fe_{0.7}Co_{0.3}$ device, while lower sensitivity values of 0.268 ± 0.007 and $0.153 \pm 0.015\ RIU^{-1}$, respectively, are observed in the Au/Fe and Au/Co transducers. Compared to Au/Co transducers, the $Au/Fe_{0.7}Co_{0.3}$ device shows about 2 times higher index sensitivity, therefore demonstrating its promising potential for chemical and biomedical sensing applications.

4. CONCLUSION

In summary, in this paper we report the enhanced TMOKE and refractive index sensitivity of Au/Fe_xCo_{1-x} bilayer MOSPR transducers. The optical and magneto-optical properties of Fe_xCo_{1-x} thin films are characterized as a function of the Fe concentrations. Both numerical simulations and experimental results show that the device sensitivity is strongly related to the composition of the magneto-optical alloy thin films. For the film compositions studied in this paper, the highest device sensitivity, of $0.306 \pm 0.008\ RIU^{-1}$, is observed in $Au/Fe_{0.7}Co_{0.3}$ transducers. This is about 2 times higher than the Au/Co transducers, and is strongly related to the enhanced magneto-optical properties of the $Fe_{0.7}Co_{0.3}$ thin films. Our study shows that the sensitivity of the MOSPR device is strongly related to the optical and magneto-optical properties of the magnetic metal thin films. The high sensitivity of the $Au/Fe_{0.7}Co_{0.3}$ MOSPR transducer makes it a promising candidate for chemical and biomedical sensing applications.

Funding. Ministry of Science and Technology of the People's Republic of China (MOST) (2016YFA0300802); National Natural Science Foundation of China (NSFC) (51522204, 61475031); Fundamental Research Funds for the Central Universities (ZYGX2014Z001); Science Foundation for Youths of Sichuan Province (2015JQO014); Doctoral Fund of Ministry of Education of China (20130185120009); Open Foundation of Key Laboratory of

Multispectral Absorbing Materials and Structures, Ministry of Education (ZYGX2013K007-5); Program for Changjiang Scholars and Innovative Research Team in University (PCSIRT).

REFERENCES

1. G. G. Nenninger, P. Tobiška, J. Homola, and S. S. Yee, "Long-range surface plasmons for high-resolution surface plasmon resonance sensors," Sens. Actuators B **74**, 145–151 (2001).
2. G. G. Nenninger, M. Piliarik, and J. Homola, "Data analysis for optical sensors based on spectroscopy of surface plasmons," Meas. Sci. Technol. **13**, 2038–2046 (2002).
3. B. Sepúlveda, A. Calle, L. M. Lechuga, and G. Armelles, "Highly sensitive detection of biomolecules with the magneto-optic surface-plasmon-resonance sensor," Opt. Lett. **31**, 1085–1087 (2006).
4. J. B. González-Díaz, A. García-Martín, G. Armelles, J. M. Clavero, A. Cebollada, and R. Clarke, "Surface magnetoplasmon nonreciprocity effects in noble-metal/ferromagnetic heterostructures," Phys. Rev. B **76**, 153402 (2007).
5. C. Clavero, K. Yang, J. R. Skuza, and R. A. Lukaszew, "Magnetic field modulation of intense surface plasmon polaritons," Opt. Express **18**, 7743–7752 (2010).
6. D. Regatos, B. Sepúlveda, D. Fariña, L. G. Carrascosa, and L. M. Lechuga, "Suitable combination of noble/ferromagnetic metal multilayers for enhanced magneto-plasmonic biosensing," Opt. Express **19**, 8336–8346 (2011).
7. K. Kämpf, S. Kübler, F. W. Herberg, and A. Ehresmann, "Magneto-optic surface plasmon resonance optimum layers: simulations for biological relevant refractive index changes," J. Appl. Phys. **112**, 034505 (2012).
8. E. Ferreiro-Vila, J. B. González-Díaz, R. Fermento, M. U. González, A. García-Martín, J. M. García-Martín, and E. M. Sandoval, "Intertwined magneto-optical and plasmonic effects in Ag/Co/Ag layered structures," Phys. Rev. B **80**, 125132 (2009).
9. T. J. Wang, K. H. Lee, and T. T. Chen, "Sensitivity enhancement of magneto-optic surface plasmon resonance sensors with noble/ferromagnetic metal heterostructure," Laser Phys. **24**, 036001 (2014).
10. J. Vlček, M. Lesňák, P. Otipka, and J. Sobota, "Magneto-plasmonic properties of Au/Fe/Au planar nanostructures: theory and experiments," Proc. Mater. Sci. **12**, 136–141 (2016).
11. M. Moradi, S. M. Mohseni, S. Mahmoodi, D. Rezvani, N. Ansari, S. Chung, and J. Akerman, "Au/NiFe magnetoplasmonics: large enhancement of magneto-optical Kerr effect for magnetic field sensors and memories," Electron. Mater. Lett. **11**, 440–446 (2015).
12. H. T. Huang, T. R. Ger, Y. R. Xu, and J. Y. Lai, "Surface plasmon induced enhancement with magneto-optical layer," J. Appl. Phys. **115**, 17E313 (2014).
13. S. Kübler, N. Müglich, and A. Ehresmann, "Magneto-optic surface plasmon resonance of Au/IrMn/Co/Au exchange biased layer systems," J. Appl. Phys. **116**, 064502 (2014).
14. D. Regatos, D. Fariña, A. Calle, A. Cebollada, B. Sepúlveda, G. Armelles, and L. M. Lechuga, "Au/Fe/Au multilayer transducers for magneto-optic surface plasmon resonance sensing," J. Appl. Phys. **108**, 054502 (2010).
15. T. Miihge, T. Zeidler, Q. Wang, C. Morawe, N. Metoki, and H. Zabel, "Structural and magnetic studies of Fe_xCo_{1-x}(001) alloy films on MgO (001) substrates," J. Appl. Phys. **77**, 1055–1060 (1995).
16. S. Višňovský, R. Lopušník, M. Bauer, J. Bok, J. Fassbender, and B. Hillebrands, "Magnetooptic ellipsometry in multilayers at arbitrary magnetization," Opt. Express **9**, 121–135 (2001).
17. J. P. Jay, E. Jêdryka, M. Wójcik, J. Dekoster, G. langouche, and P. Panissod, "On the stability of BCC Co in Co/Fe superlattices an NMR and XRD study," Z. Phys. B **101**, 329–337 (1997).
18. D. N. Tai, A. Chaiken, and T. W. Barbee, "Structural transition in Cu/Fe multilayered thin films," MRS Online Proc. Library Arch. **441**, 353–358 (2011).
19. R. S. Sundar and S. C. Deevi, "Soft magnetic FeCo alloys: alloy development, processing, and properties," Int. Mater. Rev. **50**, 157–192 (2005).
20. D. Hunter, W. Osborn, K. Wang, N. Kazantseva, J. Hattrick-Simpers, R. Suchoski, R. Takahashi, M. L. Young, A. Mehta, L. A. Benderky, S. E. Lofland, M. Wutting, and I. Takeuchi, "Giant magnetostriction in annealed $Co_{1-x}Fe_x$ thin-films," Nat. Commun. **2**, 518 (2013).
21. Y. B. Xu, Q. Y. Jin, Y. Zhai, M. Lu, Y. Z. Miao, Q. S. Bie, and H. R. Zhai, "Complex magneto-optical Kerr rotation of Fe, FeCo/Cu multilayer films," J. Appl. Phys. **74**, 3470–3474 (1993).
22. K. J. Kim, S. J. Lee, and D. W. Lynch, "Study of optical properties and electronic structure of ferromagnetic FeCo," Solid State Commun. **114**, 457–460 (2000).
23. A. K. Zvezdin and V. A. Kotov, *Modern Magnetooptic and Magnetooptical Materials* (CRC Press, 1997).